Available online at www.sciencedirect.com
ScienceDirect
International Journal of Mechanical Sciences 50 (2008) 315–327
International Journal of MECHANICAL SCIENCES
www.elsevier.com/locate/ijmecsci

# A theoretical study on the application of asymmetric rolling for the estimation of friction

P.P. Gudur, M.A. Salunkhe, U.S. Dixit*

*Department of Mechanical Engineering, Indian Institute of Technology, Guwahati 781039, India*

Received 26 May 2006; received in revised form 20 April 2007; accepted 11 June 2007
Available online 27 June 2007

**Abstract**

In this work, a method for the estimation of friction coefficient is proposed based on the asymmetric rolling operation. Asymmetry is produced by operating the lower and upper rolls at different speeds. A slab method based computer code is developed for estimating the curvature of the rolled sheet under asymmetric rolling conditions. Strain-hardening behavior of the material has been incorporated and Wanheim and Bay's friction model is employed. The developed code is used for solving the inverse problem of estimating the coefficient of friction by measuring the curvature of the rolled sheet under known operating conditions. The simulations show a good potential of the method.


*Keywords:* Cold rolling; Estimation of friction; Asymmetric rolling; Slab method; Strip curvature

## 1. Introduction

The friction between the roll and strip has a great influence on the cold rolling process. The different methods for the estimation of coefficient of friction in cold rolling process have been summarized in the book by Roberts [1]. The direct measurement of coefficient of friction involves measuring the roll pressure and/or interfacial shear stress at all points along the arc of contact in the roll bite, which is a difficult procedure. For measuring the roll pressure and interfacial shear stress, a number of transducers are inserted in one of the rolls. Seibel and Lueg [2] conducted some experiments, in which they inserted two quartz crystals in the holes drilled in an accurately made circular segment which acted as the bottom roll. One end of a metal pin was attached to the top crystal, whereas the other end was made to fit flush with the circumferential surface of the segment. During rolling, pressure was transmitted through the pin to the quartz crystals, which developed electrical charges proportional to the pressure. This method requires damaging of the surface of the rolls and is difficult to employ. Whitton and Ford [3] developed a method for measuring the friction under conditions of zero slip. In this method, during rolling, the back tension is gradually increased until the neutral point is brought to the exit plane. However, this method of applying a high back tension to the strip has the disadvantage of creating an artificial situation in the roll gap. The method requires the measurement of spindle torque, the rolling force and the slip of the strip. Estimation of the coefficient of friction is also possible under conditions of non-zero slip by measuring rolling torque, roll force and forward slip [1]. Roberts [1] has also described a method of calculating the coefficient of friction from roll force and strip material data.

In the present work, possibility of estimating the coefficient of friction by measuring the strip curvature in an asymmetric rolling process is investigated. The asymmetric situation is created by making the speeds of top and bottom roll different. A slab method of rolling analysis has been used to analyze the asymmetric rolling process. The slab method has been used widely for its simplicity and time efficient computation. Based on

*Corresponding author. Tel.: +91 361 2582657 (O), +91 361 2584657/2691036 (R); fax: +91 361 2690762.
*E-mail addresses:* uday@iitg.ernet.in, usd1008@yahoo.com (U.S. Dixit).

0020-7403/$ - see front matter © 2007 Elsevier Ltd. All rights reserved.
doi:10.1016/j.ijmecsci.2007.06.002

**Nomenclature**

| | |
|---|---|
| $b$ | material hardening coefficient |
| $c$ | height of the curved strip |
| $D$ | a constant dependent on the roll material |
| $F_u$, $F_l$ | roll force at the upper and lower rolls, respectively |
| $f$ | friction factor |
| $h$ | strip thickness at a distance $x$ from the center of the rolls |
| $h_1$, $h_2$ | inlet and exit strip thicknesses of strip |
| $h_u$, $h_l$ | the vertical distance between the $x$-axis and a point on the strip at the upper and the lower surfaces, respectively |
| $L$ | the projected contact length |
| $L_s$ | distance between the curved ends of strip |
| $l_0$, $l_1$, $l_2$ | lengths of the neutral, upper and lower fibers of a curved strip |
| $m$, $m_u$, $m_l$ | friction factor, friction factors for upper and lower rolls |
| $n$ | material hardening coefficient |
| $p_u$, $p_l$ | normal contact pressures at the upper and the lower surfaces in the roll gap |
| $R$ | radius of curvature of a strip |
| $R'$ | radius of deformed arc of contact |
| $R_{eq}$ | equivalent contact length |
| $R_u$, $R_l$ | radius of the upper and lower roll, respectively |
| $r$ | percentage reduction |
| $r_1$, $r_2$ | radius of curvature due to difference in normal strains and shear strains, respectively |
| $S_{xx1}$, $S_{yy1}$ | deviatoric components of stress for upper surface, in $x$ and $y$ directions, respectively |
| $S_{xx2}$, $S_{yy2}$ | deviatoric components of stress for lower surface, in $x$ and $y$ directions, respectively |
| $x_{nu}$, $x_{nl}$ | the locations of the upper and the lower neutral points, respectively |
| $Y_s$ | flow stress of the strip material |
| $(Y_s)_o$ | yield stress of the strip material |
| $\delta$ | the draft, i.e. difference between the initial and final thickness |
| $d\gamma_{xy1}$, $d\gamma_{xy2}$ | incremental shear strains at a point on the upper and the lower surfaces of the strip, respectively |
| $d\lambda$ | a constant in the flow rule |
| $\tilde{\varepsilon}$ | equivalent plastic strain |
| $\varepsilon_{x1}$, $\varepsilon_{x2}$ | axial strains at the upper and lower surfaces of the strip |
| $d\varepsilon_{x1}$, $d\varepsilon_{x2}$ | incremental axial strains in $x$ direction, for upper and lower surfaces, respectively |
| $\mu$ | coefficient of friction |
| $\mu_u$, $\mu_l$ | the coefficient of friction at the upper and lower surfaces |
| $\tau$ | average shear stress on the vertical side of the element |
| $\tau_u$, $\tau_l$ | frictional shear stresses at the upper and lower interfaces |
| $\sigma_u$, $\sigma_l$ | normal axial stresses at the upper and the lower rolls, respectively |

the slab method, Mischke [4] developed equations of equilibrium in asymmetric flat rolling. He has considered the entry angle of the strip in his formulation. Hawang and Tzou [5] used slab method and proposed an analytical model assuming constant friction factor between the roll and sheet. They measured rolling force and forward slip experimentally from which the friction factor was estimated. Salimi and Sassani [6] used the slab method to find the curvatures of the strip for different asymmetric conditions. Salimi and Kadkhodaei [7] used slab method to numerically calculate the rolling force and torque. Recently, Kadkhodaei et al. [8] has presented a slab method model of asymmetric rolling in which a genetic algorithm is used to obtain the plate deflection at entry to ensure free entry condition.

Apart from slab method, some other methods have also been used for analyzing the asymmetric rolling process. Pan and Sansome [9] have carried out some experiments on asymmetric rolling, in which asymmetry was created due to speed mismatch. The experimental results were compared with the upper and lower bound models. Kiuchi and Hsiang [10] used an upper bound technique for calculating the curvatures in the rolled plates. Hwang and Chen [11] have analyzed asymmetric sheet rolling process using an upper bound method, which makes use of a stream function. They predicted curvature of the rolled product and roll force and found them to be in good agreement with the experimental results. Dewhurst et al. [12] developed a simplified slip-line field solution for asymmetric hot rolling and predicted the curvature of the roll strip. They conducted some experiments on a two-high laboratory rolling mill and found some qualitative agreement between the experimental results and slip-line field model. Finite element method has also been used for the analysis of the asymmetric rolling process. Shivpuri et al. [13] studied the influence of the roll speed mismatch on the curvature of the plate using explicit time-integration elastic–plastic finite element method. They found that the strip always curls towards the roll with the lower speed. Richelsen [14] used elastic–viscoplastic finite element method to study the effect of different interfacial friction conditions on the curvature of the strip. The curvature of the plate was found to be towards the roll with highest friction. Lu et al. [15] performed a finite element simulation to study the influence of different diameters of the working rolls on the strip curvature.

As the main objective of this paper is to show the possibility of estimating the coefficient of friction by

asymmetric rolling, a slab method model of Salimi and Kadkhodaei [7] has been used instead of a rigorous finite element model. However, Salimi and Kadkhodaei [7] did not consider roll flattening and strain hardening which have been considered in the present work. At the same time in place of Coulomb's friction model or constant shear friction model, a more realistic Wanheim and Bay's friction model [16] has been incorporated in the present model.

## 2. Modeling of asymmetric rolling

Fig. 1 shows the schematic diagram of the asymmetric rolling process. In the general case, roll diameters, speeds and friction conditions at upper and lower rolls will be different. The inlet and outlet thicknesses of the strip are denoted by $h_1$ and $h_2$, respectively. The subscripts $u$ and $l$ represent upper and lower interfaces, respectively. Thus, $R_u$ and $R_l$ denote the radii of the upper and lower rolls whereas $V_u$ and $V_l$ represent the speeds of the upper and the lower roll. Without any loss of generality, assume that the speed of the lower roll is higher than that of the upper roll. In Fig. 1, the roll gap is divided into three zones. In zone I, the strip velocity is lower than the speeds of both the rolls and the frictional stresses on the upper and the lower surfaces are in the forward direction. In zone II, the strip velocity is more than the speed of the upper roll and less than the speed of the lower roll. Hence, the frictional stresses on the upper surface act in the backward direction and that on the lower surface act in the forward direction. In zone III, as the speeds of both the rolls are lower than the strip velocity, the frictional stresses at both the surfaces are in the backward direction. The contact length $L$ and the thickness $h$ of the strip at a distance $x$ from the center of the rolls can be obtained from the following relationships [7]:

$$L=\frac{\{(h_1-h_2)(2R_u+h_2-h_1)(2R_l+h_2-h_1)[2(R_u+R_l)+(h_2-h_1)]\}^{1/2}}{2(R_u+R_l+h_2-h_1)}, \tag{1}$$

$$h=h_2+\frac{x^2}{R_{eq}}, \tag{2}$$

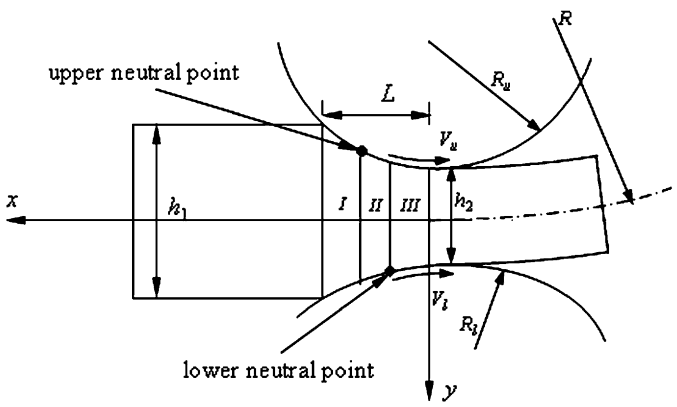


Fig. 1. The schematic diagram of asymmetric rolling.

where the equivalent radius, $R_{eq}$, is given by

$$R_{eq}=\frac{2R_uR_l}{R_u+R_l}. \tag{3}$$

### 2.1. Governing equations and solution procedure

A small slab element of length $dx$ and thickness $h$ at a distance $x$ from the center of the rolls is shown in Fig. 2. The normal and shear stresses are assumed to be distributed linearly across the thickness. $O$ is the mid-point of the right-hand side face of the element. For the equilibrium of this element, the net forces along the rolling direction, the net forces along the normal direction and the net moments of the forces about any chosen point (say $O$) should be equated to zero. This leads to the following set of equations:

$$\sum F_x=\left(\frac{p_u}{R_u}+\frac{p_l}{R_l}\right)x-\frac{x}{R_{eq}}(\sigma_u+\sigma_l)-(\tau_u+\tau_l)-\frac{h}{2}\left(\frac{d\sigma_u}{dx}+\frac{d\sigma_l}{dx}\right)=0, \tag{4}$$

$$\sum F_y=\frac{2x}{R_{eq}}\tau+(p_l-p_u)+\left(\frac{\tau_l}{R_l}-\frac{\tau_u}{R_u}\right)x+h\frac{d\tau}{dx}=0, \tag{5}$$

$$\sum M_o=h\tau+\frac{xh}{2}\left(\frac{p_l}{R_l}-\frac{p_u}{R_u}\right)+\frac{xh}{2R_u}(\sigma_u+\sigma_l)+\frac{h}{2}(\tau_u-\tau_l)-\frac{xh}{6R_{eq}}(\sigma_u+5\sigma_l)+\frac{h^2}{12}\left(\frac{d\sigma_u}{dx}-\frac{d\sigma_l}{dx}\right)=0, \tag{6}$$

where $p_u$ and $p_l$ are the normal pressures at the upper and the lower rolls, $\sigma_u$ and $\sigma_l$ are the longitudinal compressive stresses on the top and bottom of the vertical surfaces of the element, $\tau_u$ and $\tau_l$ are the interfacial shear stresses at the upper and the lower interfaces, respectively, and $\tau$ is the average shear stress acting on the vertical surface of the

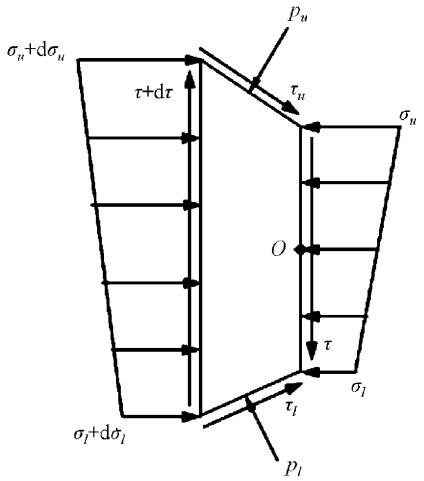


Fig. 2. A small slab element in equilibrium.

material. The interfacial shear stresses $\tau_u$ and $\tau_l$ are calculated by using Wanheim and Bay's friction model (see the appendix). Rearranging the terms in Eqs. (4) and (6), we get

$$\left(\frac{d\sigma_u}{dx}+\frac{d\sigma_l}{dx}\right)=\frac{2x}{h}\left(\frac{p_u}{R_u}+\frac{p_l}{R_l}\right)-\frac{2x}{hR_{eq}}(\sigma_u+\sigma_l)-\frac{2}{h}(\tau_u+\tau_l)=A, \tag{7}$$

$$\left(\frac{d\sigma_l}{dx}-\frac{d\sigma_u}{dx}\right)=\frac{12}{h}\tau+\frac{6x}{h}\left(\frac{p_l}{R_l}-\frac{p_u}{R_u}\right)+\frac{6x}{hR_u}(\sigma_u+\sigma_l)+\frac{6}{h}(\tau_u-\tau_l)-\frac{2x}{hR_{eq}}(\sigma_u+5\sigma_l)=B. \tag{8}$$

Assuming that the strip is in plane-strain condition and following Levy–Mises flow rule [17],

$$\tau_{xz}=\tau_{yz}=0, \qquad \sigma_z=\tfrac{1}{2}(\sigma_x+\sigma_y). \tag{9}$$

Substituting these in the von Mises criterion, we get

$$\left|\frac{\sigma_x-\sigma_y}{2}\right|=\sqrt{\frac{Y_s^2}{3}-\tau_{xy}^2}. \tag{10}$$

For small bite angle, one can write [7]

$$\sigma_u=p_u-2\sqrt{\frac{Y_s^2}{3}-\tau_u^2} \tag{11}$$

and

$$\sigma_l=p_l-2\sqrt{\frac{Y_s^2}{3}-\tau_l^2}. \tag{12}$$

For most of the strain-hardening materials, the flow stress $Y_s$ can be given by

$$Y_s=(Y_s)_0\left(1+\frac{\tilde{\varepsilon}}{b}\right)^n, \tag{13}$$

where $b$ and $n$ are hardening parameters which are material dependant and $\tilde{\varepsilon}$ is the equivalent plastic strain. Assumptions of volume constancy, plain strain and across the thickness uniform plastic strain in the thickness direction allow us to write the equivalent strain as

$$\tilde{\varepsilon}=\frac{2}{\sqrt{3}}\ln\left(\frac{h}{h_1}\right). \tag{14}$$

It is to be noted that although the present model accounts for an internal shear stress, yet in Eq. (14), the shear strain is neglected in the computation of overall strain. It was found that for the cases studied in this paper, the shear strain was limited to a maximum of 20% of overall equivalent strain in the most severe cases. This introduces less than 5% error in the estimation of flow stress because of the low value of exponent $n$. Hence, for the estimation of flow stress, the approximate equivalent strain expression given by Eq. (14) is justified. Thus, the equation for the flow stress becomes

$$Y_s=(Y_s)_0\left(1+\frac{2}{\sqrt{3}}\frac{\ln(h_1/h)}{b}\right)^n. \tag{15}$$

As the strip thickness is a function of $x$, the above expression of flow stress is also a function of $x$. Differentiating Eq. (15) we obtain

$$\frac{dY_s}{dx}=C\frac{dh}{dx}, \tag{16}$$

where

$$C=-(Y_s)_0\frac{2/\sqrt{3}n}{bh}\left(1+\frac{2}{\sqrt{3}}\frac{\ln(h_1/h)}{b}\right)^{n-1}. \tag{17}$$

Differentiating Eqs. (11) and (12) with respect to $x$, substituting these derivatives as well as Eq. (16) in Eqs. (5), (7) and (8), the following system of equations is obtained:

$$\frac{dp_u}{dx}=\frac{A-B}{2}-\frac{\tau_u}{R_u}-\frac{x}{R_u}\frac{d\tau_u}{dx}+\frac{3}{\sqrt{Y_s^2-3\tau_u^2}}\left(\frac{4Y_sC}{3R_{eq}}x-2\tau_u\frac{d\tau_u}{dx}\right), \tag{18}$$

$$\frac{dp_l}{dx}=\frac{A+B}{2}-\frac{\tau_l}{R_l}-\frac{x}{R_l}\frac{d\tau_l}{dx}+\frac{3}{\sqrt{Y_s^2-3\tau_l^2}}\left(\frac{4Y_sC}{3R_{eq}}x-2\tau_l\frac{d\tau_l}{dx}\right), \tag{19}$$

$$\frac{d\tau}{dx}=\frac{x}{h}\left(\frac{\tau_u}{R_u}-\frac{\tau_l}{R_l}\right)+\left(\frac{p_u-p_l}{h}\right)-\frac{2x}{R_{eq}}\frac{\tau}{h}, \tag{20}$$

where $A$, $B$ and $C$ are defined as per Eqs. (7), (8) and (17), respectively. These are system of three first-order ordinary differential equations in $p_u$, $p_l$ and $\tau$. To solve this system, three initial conditions are necessary. These can be obtained from the loading conditions at the exit. Using volume constancy, the positions of the two neutral points can be related by the following relationship:

$$x_{nu}=\sqrt{V_Ax_{nl}^2+R_{eq}h_2(V_A-1)}, \tag{21}$$

where $V_A$ is the ratio of the surface velocities of the lower roll to that of the upper roll, $x_{nu}$ and $x_{nl}$ are the distances of the upper and the lower neutral points from the centers of the rolls, respectively. Thus, if the location of one of the neutral points is known, from the above relation the location of the other point can be calculated easily. It is assumed that the frictional stresses between the strip and the guide rollers that are provided for the horizontal entrance of the strip are negligible and no back tension or compression to the plate is applied. Hence, no axial forces at the entry section to the plastic region exist.

In order to solve the above-mentioned initial value problem, a MATLAB function ODE45 is used in the code developed. The function ODE45 is based on fourth-order explicit Runge–Kutta method, which consists of dividing the time interval into appropriate parts called steps. It is

a one-step solver which means in computing the dependant variables at time $t_n$, it needs only the solution at time $t_{n-1}$, i.e. the values of variables at one time step before. As the roll gap gets divided into three zones as a consequence of the asymmetric rolling. Hence, the locations of the neutral points are crucial in determining the extent of each zone. The solution process consists of adjusting the location of one of the neutral points (say, lower neutral point) and solving the above mentioned initial value problem in an iterative manner. Each zone is divided into 100 equal parts. The differentials $d\tau_u/dx$ and $d\tau_l/dx$ in Eqs. (18) and (19) at $i$th point are calculated by using finite difference approximations:

$$\frac{d\tau_u}{dx}=\frac{(\tau_u)_{i-1}-(\tau_u)_{i-2}}{\Delta x} \quad \text{and} \quad \frac{d\tau_l}{dx}=\frac{(\tau_l)_{i-1}-(\tau_l)_{i-2}}{\Delta x}. \tag{22}$$

The difficulty of getting the values of the differentials for the first two points by the above formula is tackled by expressing $d\tau_u/dx$ and $d\tau_l/dx$ as $d\tau_u/dx=\mu dp_u/dx$ and $d\tau_l/\mu dp_l/dx$, where $\mu$ corresponds to equivalent Coulomb's coefficient of friction. This is a valid assumption as the pressure at these two points is low for which the Wanheim and Bay's model reduces to Coulomb's model [16]. The neutral point position is adjusted in such a way that the mean axial normal stress $(\sigma_u+\sigma_l)/2$ at the entry section becomes equal to zero. This task is carried out by employing bisection method [18]. The first step consists of assuming lower neutral point $x_{nl}$ to be placed at two extreme positions, one near the entry section and other near the exit section. The position of the upper neutral point $x_{nu}$ can be calculated by Eq. (21) and the roll gap gets divided into three zones. For each case, the value of the mean axial stress at inlet section is calculated. If $x_{nl}$ is near the exit section, we get a negative value for the mean axial stress, corresponding to the presence of a back tension. If $x_{nl}$ is near the inlet section, we get a positive value. Thus, if we search in between these two extreme values, we can get the true locations of the neutral points corresponding to zero mean axial stress. The next step consists of halving the search interval and solving the problem by placing the lower neutral point $x_{nl}$ exactly at the middle of the initial interval and calculating mean normal stress for this case. Depending on its value, one of the two intervals is eliminated. Again, the remaining interval is divided into two equal parts and the procedure is repeated in an iterative manner till almost zero value of the mean axial normal stress at the inlet section is obtained. The solution at this stage will be the solution of our problem. Thus, the values of $p_u$, $p_l$, and $\tau$ at all the points are obtained. If the contact angle of the rolls and that of the plate is small, the roll force per unit width can be calculated as [7]

$$F_u=\int_0^L\left(p_u+\frac{x}{R_u}\tau_u\right)dx \quad \text{and} \quad F_l=\int_0^L\left(p_l+\frac{x}{R_l}\tau_l\right)dx. \tag{23}$$

During rolling process the rolls get elastically deformed. This roll flattening effect is taken into consideration using Hitchcock's formula [19] in which the ratio of the radius of the deformed arc of contact to the roll radius is given by

$$\frac{R'}{R}=\left(1+\frac{F}{D\delta}\right), \tag{24}$$

where $F$ is the roll force and $\delta=h_1-h_2$ is the "draft". The constant $D$ depends on the material of the rolls, its value for steel rolls being $4.62\times10^4\,\mathrm{MN/m^2}$. The radius of the deformed arc of contact is found in an iterative manner. In the first iteration, no roll deformation is assumed and the governing differential equations (18)–(20) are solved. The roll forces on both the roll are obtained using Eq. (23). Knowing the force values, radii of deformed portion of the rolls are obtained from Eq. (24). Treating these values as undeformed radii, Eqs. (18)–(20) are solved to get new force values. Putting these force values in Eq. (24), new radii of deformed arc of contact are obtained. This procedure is repeated in an iterative manner till the roll-radii converge. The converged solution is used for calculating the strip curvature. Taking moment about the center of roll, the rolling torque per unit width is given by,

$$T_u=\int_0^L xp_u\,dx \quad \text{and} \quad T_l=\int_0^L xp_l\,dx. \tag{25}$$

It is to be mentioned that Hitchcock's formula is incapable of estimating roll deformation for rolling of thin and hard strips particularly at low reduction. However, for the cases examined in this paper, Hitchcock's formula is appropriate. This is supported by the work of Chandra and Dixit [20], who have estimated the roll deformation by treating the roll as an elastic half space and using a theory of elasticity solution. They found that for moderate strip thickness, reduction, flow stress of the material and friction, their model provides almost same results as the model of Dixit and Dixit [21], which uses Hitchcock's model. A more accurate roll deformation model will be needed for the studying the rolling of thin and hard strips at low reduction.

### 2.2. Calculation of strip curvature

The asymmetry in the rolling process imparts an undesirable curvature to the outgoing strip. There are two different types of effects that contribute to this curvature. The first is due to the difference in the axial strains at the upper and the lower surfaces and the second is due to the difference in the shear strains at the upper and the lower surfaces. The total curvature will be equal to the summation of the curvatures due to these two effects. The analysis procedure is somewhat similar to that of Salimi and Sassani [6].

#### 2.2.1. Strip curvature due to difference in axial strains

Consider that the strip undergoes a curvature as shown in Fig. 3. This type of curvature (convex upward) is

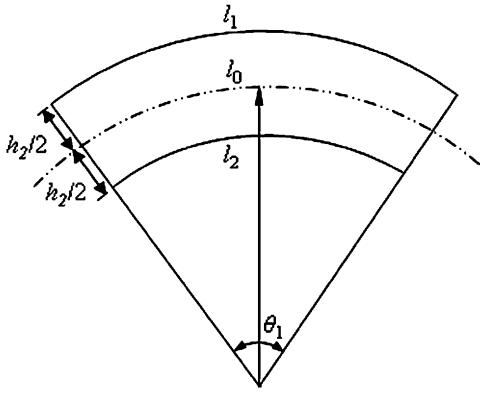


Fig. 3. The strip curvature due to difference in axial strains.

considered negative in the sign convention adopted. Let $l_1$, $l_2$, and $l_0$ be the lengths of the upper, lower and the neutral fibers.

From the geometry of the figure we can write

$$\frac{1}{r_1} = -\frac{1}{h_2}\left(\frac{l_1 - l_2}{l_0}\right) = -\frac{1}{h_2}(\varepsilon_{x1} - \varepsilon_{x2}), \tag{26}$$

where $r_1$ is the radius of curvature due to difference in axial strains and $\varepsilon_{x1}$ and $\varepsilon_{x2}$ are the axial strains at the upper and lower surfaces, respectively. The incremental strain in the $y$ direction is given by

$$\mathrm{d}\varepsilon_y = -\frac{\mathrm{d}h}{h} = -\frac{2x}{hR_{eq}}. \tag{27}$$

According to the flow rule, the incremental strain in the $x$ direction for the upper surface can be given by

$$\mathrm{d}\varepsilon_{x1} = s_{xx1}\frac{\mathrm{d}\varepsilon_y}{s_{yy1}} = s_{xx1}\,\mathrm{d}\lambda, \tag{28}$$

where $\mathrm{d}\lambda$ is a constant and $s_{xx1}$ and $s_{yy1}$ are the deviatoric components of stress in $x$ and $y$ directions on the upper surface. Assuming the incremental strain in $y$ direction to be uniform the constant $\mathrm{d}\lambda$ can be calculated as

$$\mathrm{d}\lambda = \frac{\mathrm{d}\varepsilon_y}{s_{yy}}, \tag{29}$$

where $s_{yy}$ is the average value of the deviatoric component in $y$ direction. Substituting $\mathrm{d}\lambda$ in Eq. (28), the incremental strain $\mathrm{d}\varepsilon_{x1}$ can be obtained. The axial strain $\varepsilon_{x1}$ can be calculated by integrating $\mathrm{d}\varepsilon_{x1}$ from 0 to $L$. Similarly, $\varepsilon_{x2}$ can be found and using Eq. (26) the curvature due to difference in axial strains can be found.

### 2.2.2. Strip curvature due to difference in shear strains

As the material undergoes deformation in the roll gap, the strip adopts a curvature due to the differential shear strains also. Employing the flow rule, the incremental shear strain at any point for the upper and lower surfaces is given by

$$\mathrm{d}\varepsilon_{xy1} = s_{xy1}\frac{\mathrm{d}\varepsilon_{y1}}{s_{yy1}} = \tau_u\frac{\mathrm{d}\varepsilon_{y1}}{s_{yy1}}, \tag{30}$$

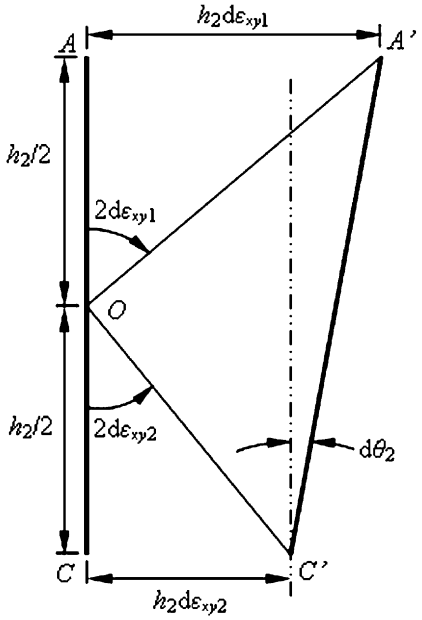


Fig. 4. Strip curvature due to difference in shear strains.

$$\mathrm{d}\varepsilon_{xy2} = s_{xy2}\frac{\mathrm{d}\varepsilon_{y2}}{s_{yy2}} = \tau_l\frac{\mathrm{d}\varepsilon_{y2}}{s_{yy2}}. \tag{31}$$

Fig. 4 shows the distortion of a vertical plane of strip due to shear strains in highly exaggerated manner. Let the points $A$ and $C$ of a vertical element get displaced to $A'$ and $C'$, respectively. The small rotation $\mathrm{d}\theta_2$ caused due to the difference in these incremental strains can be given as

$$\mathrm{d}\theta_2 = \frac{h_2\,\mathrm{d}\varepsilon_{xy1} - h_2\,\mathrm{d}\varepsilon_{xy2}}{h_2} = \mathrm{d}\varepsilon_{xy1} - \mathrm{d}\varepsilon_{xy2}. \tag{32}$$

The total angle subtended by the strip due to the differential shear strain can be calculated as

$$\theta_2 = \int_0^L (\mathrm{d}\varepsilon_{xy1} - \mathrm{d}\varepsilon_{xy2}). \tag{33}$$

Therefore the strip curvature due to difference in the shear strains is given by

$$\frac{1}{r_2} = -\frac{\int_0^L (\mathrm{d}\varepsilon_{xy1} - \mathrm{d}\varepsilon_{xy2})}{L}. \tag{34}$$

The total curvature to the strip will be the summation of the curvature due to the difference in the axial strains and curvature due to the difference in the shear strains. Thus, the resultant radius of curvature ($R$) is given by

$$R = \frac{r_1 r_2}{r_1 + r_2}. \tag{35}$$

## 3. Results of the model

The present model is compared for the roll force and roll torque values with the experimental results of Hwang and Tzou [5] as well as analytical results obtained by Salimi and

Kadkhodaei [7]. In the case of curvature, results are compared with the experimental results of Buxton and Browning [22], Kennedy and Slammer [23] and finite element analysis results of Shivpuri et al. [13].

### 3.1. Rolling force and rolling torque

The roll force calculated by present model for both asymmetric and symmetric cases are shown in Fig. 5. In Fig. 5(a), the roll deformation is taken into consideration according to the Hitchcock's formula and Wanheim and Bay's friction model is used. For the present model, the coefficients of friction values correspond to equivalent Coulomb's coefficient values, i.e. the ratio of normal traction to shear traction at low values of roll pressure. It can be seen that the roll force calculated from the present model is higher than that given by Salimi and Kadkhodaei [7]. This is mainly due to the roll flattening effect. It was observed that for the roll pressure values observed for the cases studied, the Coulomb's model and Wanheim and Bay's model differ only slightly. Also, it is clear that the roll force in asymmetrical rolling is slightly lower than that of symmetrical rolling. Fig. 5(b) shows the effect of input thickness on the roll force when the strain-hardening behavior of the material is incorporated in the present model. Comparing Fig. 5(a) and (b), it is clear that strain hardening of material has a significant effect on the rolling force.

The experimental values of roll force [5] have been compared with the results of the present model in Fig. 6(a) and (b) for different inlet strip thicknesses. In Fig. 6, asymmetry is caused due to speed mismatch only whereas in Fig. 7, the asymmetry is caused due to speed mismatch as well as due to different roll radii. It is seen that in all cases, the predictions by the present model are in a close agreement with the experimental results. It is to be mentioned that for the sake of comparison, a constant friction factor model was incorporated in the present model. In the constant friction factor model, the shear stresses at the roll–strip interface is given by

$$\tau = m\frac{Y_s}{\sqrt{3}}, \tag{36}$$

where $m$ is the friction factor.

Fig. 8 shows the roll force values for the case in which asymmetry is created due to different friction coefficients at the upper and lower rolls as well as roll speed mismatch.

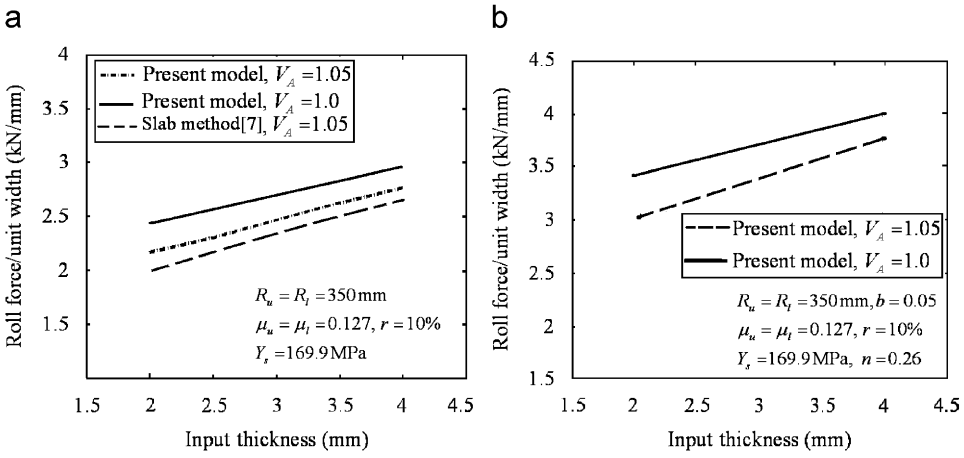


Fig. 5. Effect of input thickness on roll force: (a) non-hardening and (b) with strain hardening.

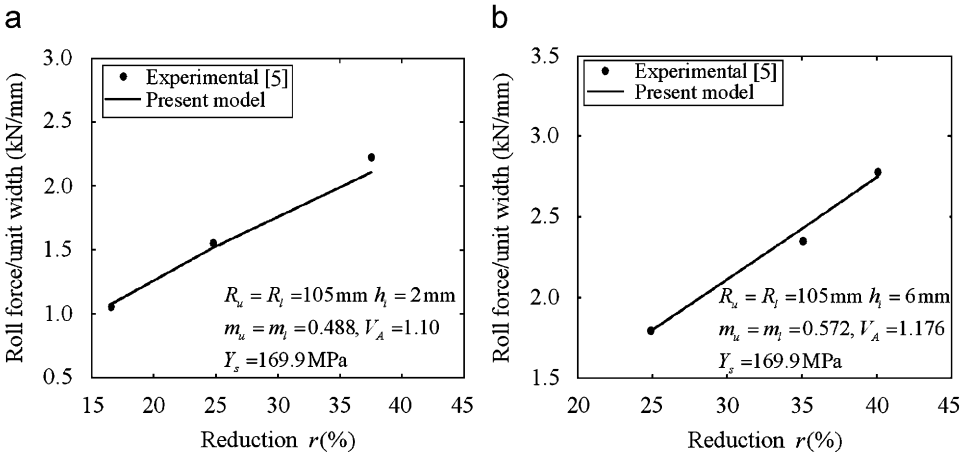


Fig. 6. Comparison of experimental and analytical roll force for speed mismatch: (a) $h_i = 2$ mm and (b) $h_i = 6$ mm.

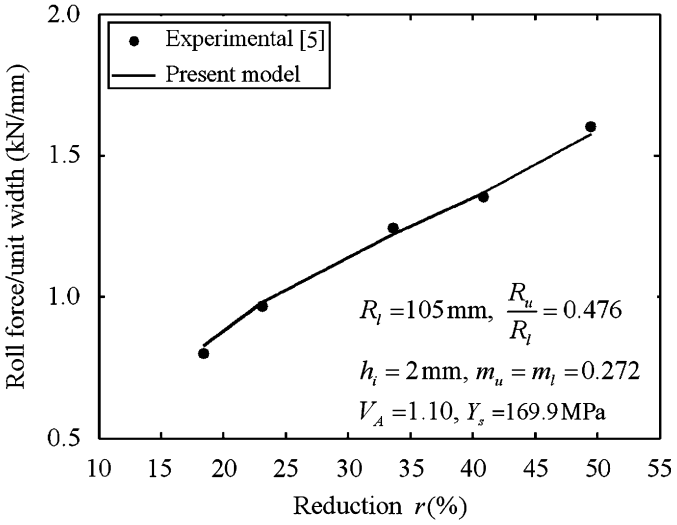


Fig. 7. Comparison of experimental and analytical roll force for different roll radii.

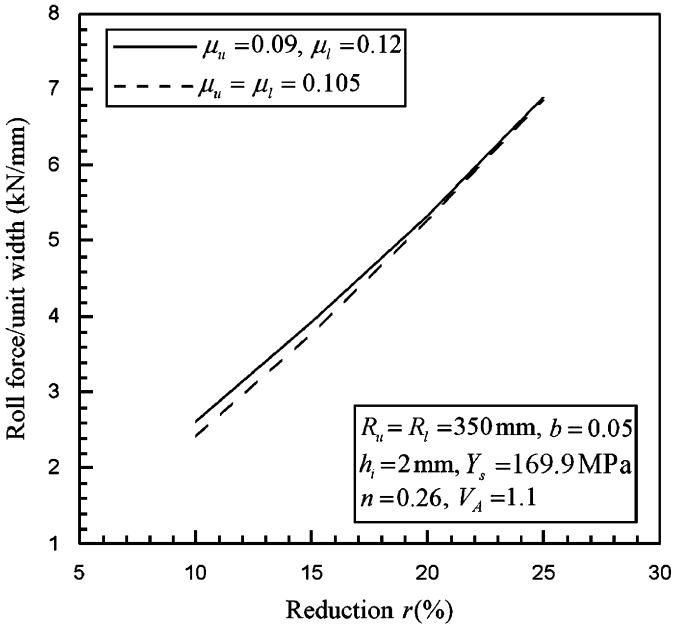


Fig. 8. Variation of roll force with reduction for different and same frictions on upper and lower rolls.

These roll forces are compared with the roll force values obtained by taking the average value of friction coefficient. It is observed that there is no significant difference in the roll force values when an average value of coefficient of friction is used. Thus, the lowering of roll force is mainly due to roll speed mismatch. It is to be noted that the present method assumes the constancy of volume across any section. The neutral points in the upper and lower rolls are related to the velocity ratio. For the velocity ratio of 1, the present model provides same location of neutral point irrespective of the asymmetry due to friction. However, a rigid plastic finite element model of asymmetric rolling [24] indicates only slight difference in the location of neutral points due to friction mismatch.

The roll force and roll torque of the present model has also been compared with the results of the finite element analysis of asymmetric rolling [24]. Roll force and roll torque of the present method are in fairly good agreement with the finite element analysis. For a typical case of speed mismatch, the results have been shown in Fig. 9.

Fig. 10 shows the effect of friction on the roll torque. In Fig. 10(a), the roll flattening along with Wanheim and Bay's friction model is incorporated. In addition to it, the strain-hardening effect has been incorporated in Fig. 10(b). It is observed that in Fig. 10, the asymmetry due to roll speed mismatch reduces not only the roll force but also roll torque. Although the internal power dissipation due to plastic deformation increases due to increased shear strains in asymmetric rolling, the friction power dissipation reduces drastically. As a result, total power gets reduced, leading to reduced torque requirement. For the case of $R_u = R_l = 350\,\text{mm}$, $\mu_u = \mu_l = 0.14$, $Y_s = 169.9\,\text{MPa}$, $h_i = 4\,\text{mm}$, $r = 10\%$, Table 1 shows the total power dissipations with corresponding frictional power dissipation and plastic deformation power dissipation. The power dissipation due to friction is computed as

$$P_f = \int_{\Gamma_u} \tau_u \left|\frac{1}{h_n} - \frac{1}{h}\right| V_2 h_2 \, d\Gamma_u + \int_{\Gamma_l} \tau_l \left|\frac{1}{h_n} - \frac{1}{h}\right| V_2 h_2 \, d\Gamma_l, \quad (37)$$

where $h_n$ is the strip thickness at the neutral point and $\Gamma_u$ and $\Gamma_l$ are the upper and lower roll–strip interface, respectively. The total power is calculated by multiplying the roll torque by the angular velocity of the roll. The plastic deformation power dissipation is obtained by subtracting the frictional power dissipation from the total power. It is observed that as the asymmetry due to roll speed mismatch increases, the frictional power dissipation reduces rapidly, whereas plastic deformation power dissipation increases with slightly slower rate. The net effect is that with increasing roll speed mismatch, the total power keeps reducing. When the asymmetry is due to friction mismatch, there seems to be no significant reduction in frictional power dissipation.

### 3.2. The roll pressure distribution

Fig. 11 shows the pressure distribution on the two roll surfaces as well as the mean pressure distribution for both symmetric and asymmetric cases. Similar to that obtained by Salimi and Kadkhodaei [7], for a asymmetry of $V_A = 1.05$, the pressure distribution on the work rolls have more than one relative maximum and the global maximum position is not located at any of neutral points.

### 3.3. Prediction of the strip curvature

Fig. 12 shows that the effect of roll speed ratio upon the strip curvature index. The strip curvature index is the ratio of length of the top surface of the sheet to the length of the

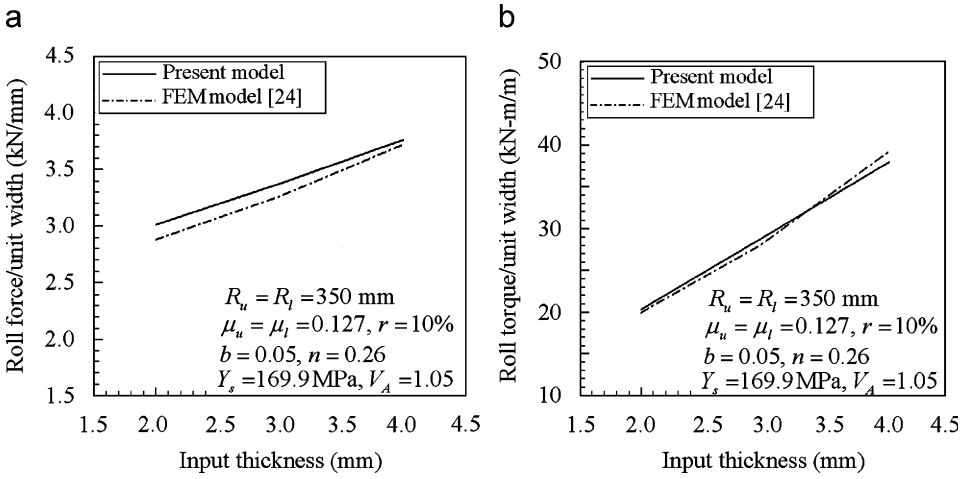


Fig. 9. Comparison of slab method with FEM analysis for speed mismatch: (a) roll force and (b) roll torque.

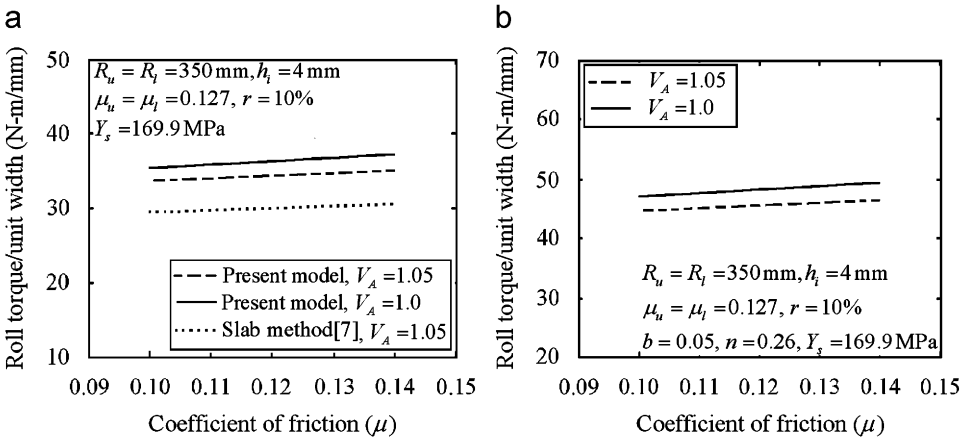


Fig. 10. Effect of coefficient of friction on roll torque: (a) non-hardening and (b) with strain hardening.

Table 1
Comparison of plastic deformation and frictional power for symmetric and asymmetric rolling

| $V_A$ | Total power (kW) | Plastic deformation power (kW) | Frictional power (kW) |
|---|---|---|---|
| 1.0 | 145.4206 | 79.0926 | 65.7816 |
| 1.01 | 131.5268 | 89.9389 | 41.5886 |
| 1.02 | 129.7112 | 96.1934 | 33.5953 |
| 1.05 | 126.0392 | 112.6071 | 13.4365 |

bottom surface of the sheet. It is denoted as $K$

$$K = \frac{R - h_2/2}{R + h_2/2}, \tag{38}$$

where $R$ is the resultant radius of curvature described in Eq. (35). The experimental results of Buxton and Browning [22], Kennedy and Slammer [23] and finite element analysis results of Shivpuri et al. [13] are compared with the present analysis. It is observed that results of the present model are in good agreement with the FEM results of Shivpuri et al. There is a good qualitative agreement with the experimental results too. The variation with the experimental results may be due to statistical variation in material parameters, error in the measurement of speed ratio and due to the use of constant friction factor model. Moreover, the experimental results pertain to hot rolling, whereas the results of present model as well as FEM model of Shivpuri et al. have been obtained without considering the thermal effects.

The effect of the asymmetry on the curvature of the strip is studied in this section. Fig. 13 shows the effect of input thickness on the curvature of the strip for different speed ratios. In the simulations, the lower roll was operated at higher speed as compared to the upper roll. The radius of curvature is always positive which indicates that the strip curls towards the upper roll, according to the adopted sign convention. It can be seen that the speed ratio has a significant effect on the curvature of the strip. Even for a small speed mismatch, the noticeable curvature can be seen. Shivpuri et al. [13] also observed the same trend in their study. As expected, the curvature goes on decreasing as the initial strip thickness is increased. It has also been observed that for an asymmetry due to friction differential, the strip always curls towards the roll having higher friction, which is in agreement with the observation of Richelsen [14].

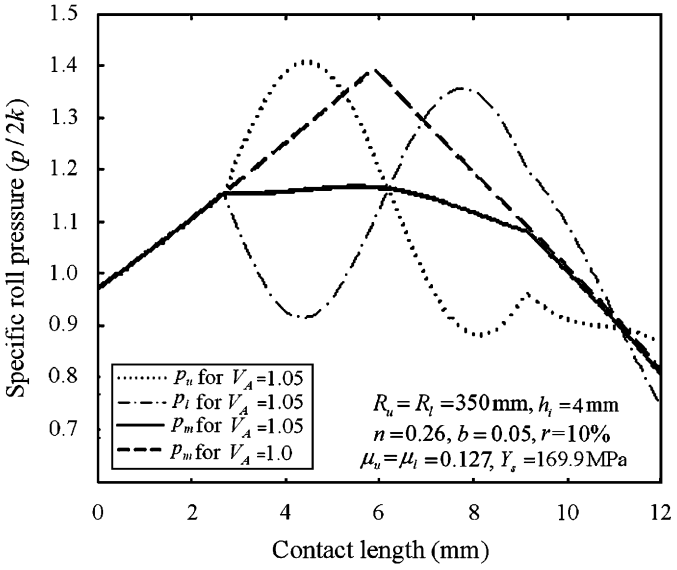


Fig. 11. The roll pressure distribution considering strain hardening.

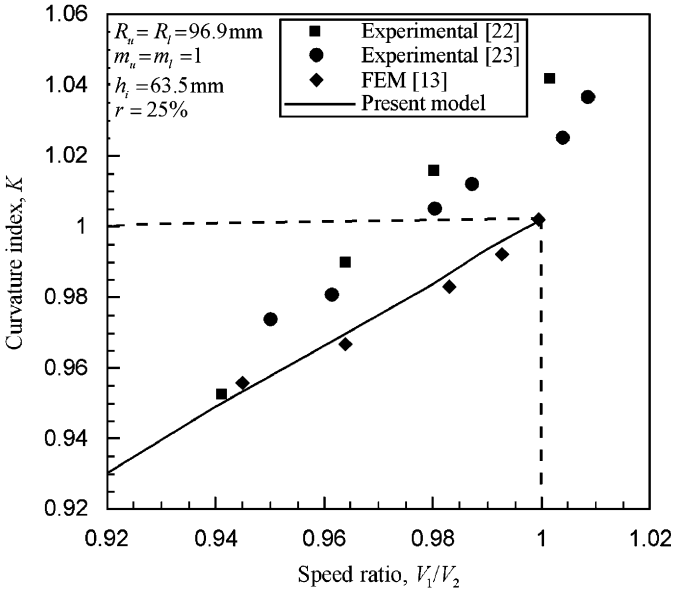


Fig. 12. Comparison of experimental, finite element analysis and present method for strip curvature index.

Fig. 14 shows the effect of the coefficient of friction on the radius of curvature for different initial thicknesses. The speed ratio considered is 1.05 and the asymmetry is due to speed mismatch only. It can be seen that as the coefficient of friction increases the curvature also goes on increasing. It is this observation, on which the present method to estimate the coefficient of friction is based.

Fig. 15 shows the effect of speed ratio on the radius of curvature of the strip for different degrees of reduction. It can be seen that the curvature goes on increasing when the speed ratio is increased. The curvature for a reduction of 20% is slightly greater than that of 10% but at 30% reduction the curvature is less than that of 10%. The curvature is always found to be positive and hence towards the slower rotating upper roll.

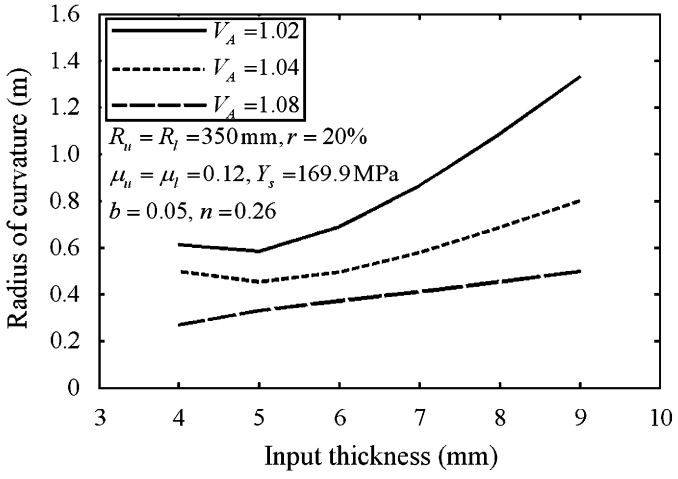


Fig. 13. Effect of input thickness on the radius of curvature for different speed ratio.

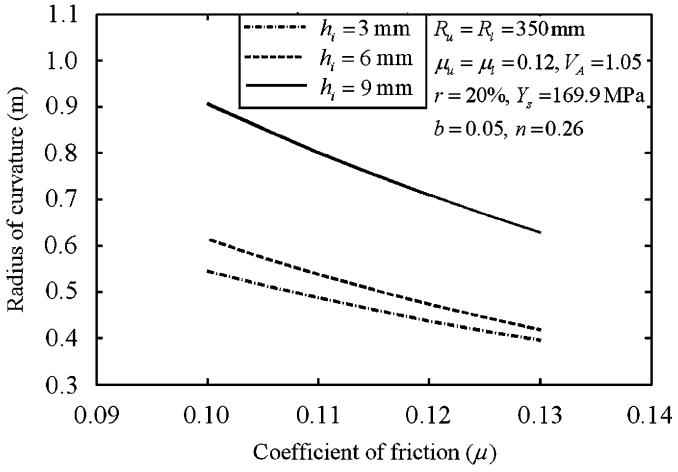


Fig. 14. Effect of coefficient of friction on the radius of curvature.

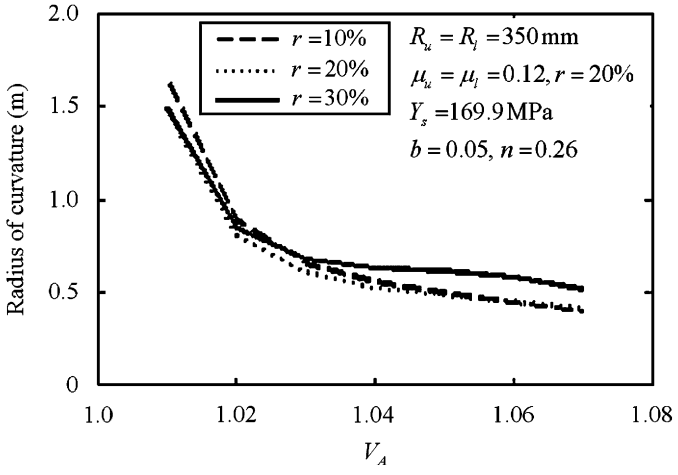


Fig. 15. Effect of $V_A$ on the radius of curvature for different reductions.

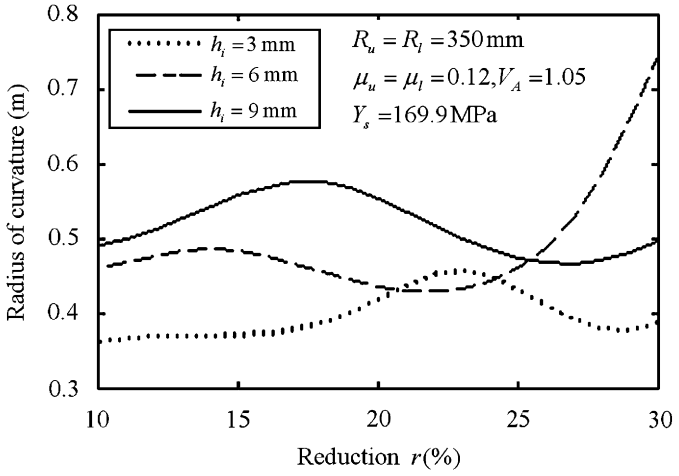


Fig. 16. Effect of percentage reduction on the radius of curvature.

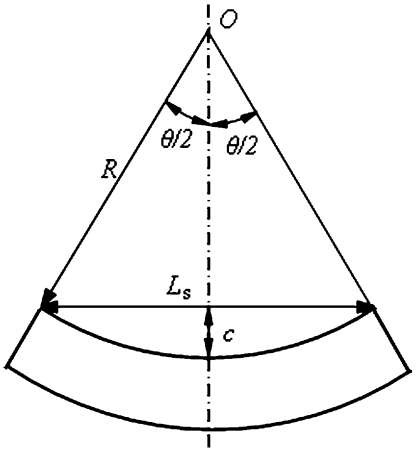


Fig. 17. Geometry of a curved strip.

Table 2
Effect of roll flattening on the strip curvature for a case of $R_u = R_l = 350$ mm, $\mu_u = \mu_l = 0.127$, $Y_s = 169.9$ MPa, $h_i = 4$ mm, $r = 20\%$

| Speed ratio, $V_A$ | Radius of curvature (m) | |
|---|---|---|
| | With roll flattening | Without roll flattening |
| 1.01 | 1.9807 | 1.8397 |
| 1.03 | 0.6647 | 0.6176 |
| 1.05 | 0.4648 | 0.4327 |

Fig. 16 shows the effect of percentage reduction on the radius of curvature for different initial strip thicknesses. It can be seen that the curvature behavior is different for different input thicknesses. At the higher reductions, the curvature is seen to decrease.

Lastly, the effect of roll flattening on the curvature of the rolled product is studied. For a few typical cases, Table 2 shows that without considering roll flattening, curvature is overestimated. Thus, roll deformation plays a significant role on the curvature.

## 4. Inverse problem: determination of coefficient of friction

This section describes the inverse problem of estimating the coefficient of friction. The curvature of the strip in the asymmetric rolling depends on the coefficient of friction for a given set of rolling conditions. This fact can be used to estimate the coefficient of friction between the rolls and the strip in symmetric rolling situation. This consists of creating an asymmetry due to speed mismatch and measuring the curvature of the emerging strip. Employing a reverse procedure, the obtained curvature is then searched by using bisection method [18] between the upper and lower estimates to obtain the value of the coefficient of friction.

Let $R$ be the measured radius of curvature, $\mu^*$ be the coefficient of friction to be estimated, $R_1$ and $R_2$ be the radii of curvature corresponding to the lower ($\mu_1$) and upper estimates ($\mu_2$) of friction, respectively. The radius of curvature is found to decrease with increasing coefficient of friction. The procedure consists of calculating the radius of curvature for a coefficient of friction, $\mu_m = (\mu_1 + \mu_2)/2$. Let this value of radius of curvature be equal to $R_m$. If $R_m > R$, then $\mu^*$ must be lying between $\mu_m$ and $\mu_2$, otherwise $\mu^*$ lies between $\mu_m$ and $\mu_1$. Again, the new limits are set and the procedure is repeated in iterative manner till the required accuracy is obtained.

The value of the radius of curvature can be calculated by using the following relation [25]:

$$R = \frac{4c^2 + L_s^2}{8c}, \tag{39}$$

where $L_s$ and $c$ are defined as shown in Fig. 17. It is obvious that the value of radius of curvature depends on the accuracy to which $c$ and $L_s$ are calculated. Assuming that typically the value of $L_s$ will be less than 0.3 m to accommodate the strip in a measuring table, and $c$ to be more than 2 mm for ensuring proper accuracy in its measurement the radius of curvature should be less than 5.6 m. The speed mismatch should be decided accordingly.

A few computer simulations were carried out for this method. The upper and lower roll radii are fixed at 350 mm. The material for the sheet to be rolled is assumed to be aluminum. An asymmetry in speed mismatch, of the order of $V_A = 1.01$–$1.02$ is created. The parameters varied are coefficient of friction and percentage reduction. The lower and upper estimates used for the coefficient of friction are $\mu_1 = 0.02$ and $\mu_2 = 0.15$, respectively. Table 3 shows the results of the simulation.

The sixth column of Table 3 shows the estimated values of the coefficient of friction from the inverse problem. Generally, 8–10 iterations of the bisection method are required to get the coefficient of friction with an accuracy of $5 \times 10^{-4}$. There may be some difficulty in estimating the lower values of coefficient of friction. At these values, a very less amount of curvature is obtained that may be

Table 3
Results of computer simulation ($Y_s = 169.9$ MPa, $b = 0.05$, $n = 0.26$)

| $h_i$ (mm) | $r$ (%) | $V_A$ | Assumed coefficient of friction | Radius of curvature, $R$ (m) | Estimated coefficient of friction, $\mu$ |
|---|---|---|---|---|---|
| 4 | 10 | 1.02 | 0.04 | 3.692 | 0.03999 |
| 4 | 20 | 1.01 | 0.08 | 1.481 | 0.08001 |
| 4 | 20 | 1.01 | 0.12 | 0.868 | 0.12002 |

difficult to measure accurately. By increasing the speed mismatch, a higher value of curvature can be obtained. However, this may take the lower neutral point out of the contact length for lower values of friction. This problem may be solved by increasing $L_s$ that in turn will yield a higher value of $c$.

## 5. A comment on the sensitivity and accuracy of the proposed method

The method proposed in the previous section assumes that the coefficient of friction is same for both the upper and lower rolls. Also, the required parameters can be measured accurately. In practice, there are two major problems. First, the accurate estimation of material parameters may be difficult; second, the friction coefficient at the upper and lower rolls may be different. The initial and final thicknesses of the strip can be measured accurately. Thus, the actual obtained reduction can always be found out.

In order to study the sensitivity of curvature, a neural network model was fitted to obtain the functional relationship between the curvature and rolling parameters. The details of neural network model are not presented here for the sake of brevity. However, it was observed that the curvature of the rolled product is insensitive to flow stress and material hardening constants. This is because the curvature mainly depends on the plastic strains, which are almost independent on material parameters. This is supported by the finite element analyses of rolling and wire-drawing [26,27], where it is observed that strain-distribution patterns practically remains unaffected by material parameters. Thus, the first problem mentioned in the previous paragraph gets resolved.

There may be the situation that one gets the same curvature as obtained by a particular friction coefficient in the case when the friction coefficients are different for upper and lower rolls. However, it will happen at a particular speed ratio $V_A$. If the speed ratio is changed, both the situations will provide different curvature. For example, Table 4 shows a typical case of this type. Here, at $V_A = 1.04$, the two different friction situations are providing same curvature, however, they provide different curvatures at $V_A = 1.02$. Thus, the second problem mentioned in the first paragraph of this section may be resolved by carrying out the experiments at two or more speed ratios. Similarly, it may also be possible to measure the friction coefficients for the cases of different friction coefficients on the lower and upper roll. Development of a robust friction identification for this purpose and fine tuning with the experimental data is left for future work.

Table 4
Radius of curvature prediction for different friction and speed ratio ($R_u = R_l = 350$ mm, $Y_s = 169.9$ MPa, $h_i = 7$ mm)

| $\mu_u$ | $\mu_l$ | Radius of curvature, $R$ (m) | |
|---|---|---|---|
| | | $V_A = 1.04$ | $V_A = 1.02$ |
| 0.10 | 0.10 | 0.9165 | 1.1996 |
| 0.04 | 0.121 | 0.9162 | 0.9239 |

## 6. Conclusion

This work presents a methodology to estimate the coefficient of friction from the asymmetric rolling process. A code based on slab method formulation has been developed for estimating the curvature of the rolled sheet under asymmetric rolling conditions. The strain-hardening behavior of the material and the roll flattening effect are incorporated along with Wanheim and Bay's friction model. It has been found that strain hardening and roll flattening have significant effect on the overall rolling process. When the asymmetry due to speed mismatch is considered it has been found that the strip curls towards the slower rotating roll, the magnitude of the curvature being dependant on the value of friction. The inverse problem of finding out the coefficient of friction given the radius of curvature is solved using the bisection method. Simulation results indicate a good potential of the method.

## Acknowledgments

Authors are thankful to the anonymous reviewers for many valuable suggestions.

## Appendix. Wanheim and Bay's friction model

In a non-sticking zone, the general relationship between interfacial shear stress and roll pressure can be expressed as

$$\tau = \mu p. \tag{A.1}$$

In the case of Coulomb model, the coefficient of friction, $\mu$ is assumed to be constant. However, in the case of Wanheim and Bay's model, $\mu$ depends on the normal

pressure. The Wanheim and Bay's model is as follows [16]:

$$\tau = \begin{cases} \mu p & \text{for } p \leqslant p', \\ \tau' + (fY_s/\sqrt{3} - \tau')\left(1 - \exp\left(\dfrac{(p' - p)\tau'}{(fY_s/\sqrt{3} - \tau')p'}\right)\right) & \text{for } p > p', \end{cases} \tag{A.2}$$

where $\tau'$ and $p'$ are the tangential and the normal stresses at the limit of proportionality given by [28]

$$\frac{\tau'}{Y_s} = \frac{1 - \sqrt{1 - f}}{\sqrt{3}}, \tag{A.3}$$

$$\frac{p'}{Y_s} = \frac{1 + (\pi/2) + \cos^{-1} f + \sqrt{1 - f^2}}{\sqrt{3}(1 + \sqrt{1 - f})} \tag{A.4}$$

and $f$ is the friction factor related to the coefficient of friction by the relation

$$\mu = \frac{f}{1 + (\pi/2) + \cos^{-1} f + \sqrt{1 - f^2}}, \tag{A.5}$$

where $Y_s$ is the flow stress of the strip material.

## References


[1] Roberts WL. Cold rolling of steel. New York: Marcel Dekker, Inc.; 1978.

[2] Siebel E, Lueg W. Investigations into the distribution of pressure at the surface of the material in contact with rolls. Mitteilungen Kaiser-Wilhelm Institut Eisenforschung 1933;15:1.

[3] Whitton PW, Ford H. Surface friction and lubrication in cold strip rolling. In: "Research on the rolling of strip": a symposium of selected papers, 1948–1958, The British Iron Steel Research Association.

[4] Mischke J. Equations of strip equilibrium during asymmetrical flat rolling. Journal of Materials Processing Technology 1996;61:382–94.

[5] Hwang YM, Tzou GY. Analytical and experimental study on asymmetrical sheet rolling. International Journal of Mechanical Sciences 1997;39:289–303.

[6] Salimi M, Sassani F. Modified slab analysis of asymmetrical plate rolling. International Journal of Mechanical Sciences 2002;44: 1999–2023.

[7] Salimi M, Kadkhodaei M. Slab analysis of asymmetrical sheet rolling. Journal of Materials Processing Technology 2004;150:215–22.

[8] Kadkhodaei M, Salimi M, Poursina M. Analysis of asymmetrical sheet rolling by a genetic algorithm. International Journal of Mechanical Sciences 2007;4:622–34.

[9] Pan D, Sansome DH. An experimental study of the effect of roll speed mismatch on the rolling load during the cold rolling of the strip. : Journal of Mechanical Working Technology 1982; 6:361–77.

[10] Kiuchi M, Hsiang S. Analytical model of asymmetrical rolling process of sheet. In: Proceedings of the 14th NAMRC. Minneapolis: Society of Manufacturing Engineers; 1986. p. 348.

[11] Hwang YM, Chen TH. Analysis of asymmetrical sheet rolling by stream function method. JSME, International Journal, Series A 1996;39:598–605.

[12] Dewhurst P, Collins IF, Johnson W. A theoretical and experimental investigation into asymmetrical hot rolling. International Journal of Mechanical Sciences 1974;16:389–97.

[13] Shivpuri R, Chou PC, Lau CW. Finite element investigation of curling in non-symmetric rolling of flat stock. International Journal of Mechanical Sciences 1988;30:625–35.

[14] Richelsen A. Elastic plastic analysis of the stress and strain distributions in asymmetric rolling. International Journal of Mechanical Sciences 1997;39:1199–211.

[15] Lu J-S, Harrer O-K, Schwenzfeier W, Fischer FD. Analysis of the bending of the rolling material in asymmetrical sheet rolling. International Journal of Mechanical Sciences 2000;42:49–61.

[16] Wanheim T, Bay N. A model for friction in metal forming processes. Annals of CIRP 1978;27:189–94.

[17] Chakrabarty J. Theory of plasticity. New York: McGraw-Hill; 1987.

[18] Kreyszig E. Advanced engineering mathematics. New York: Wiley; 1999.

[19] Hitchcock H. Roll neck bearings. New York: App. I. ASME; 1935.

[20] Chandra S, Dixit US. A rigid-plastic finite element analysis of temper rolling process. Journal of Materials Processing Technology 2004; 152:9–16.

[21] Dixit US, Dixit PM. A finite element analysis of flat rolling and applications of fuzzy set theory. International Journal of Machine Tools and Manufacture 1996;36:947–69.

[22] Buxton SA, Browning SC. Turn-up and turn-down in hot rolling: a study on a model mill using plasticine. Journal of Mechanical Engineering Sciences 1972;14:245.

[23] Kennedy GE, Slamar F. Turn-up and turn-down in hot rolling. Iron and Steel Engineer 1958:35–71.

[24] Salunkhe MA. Analysis of cold flat asymmetric rolling process. M Tech thesis, Indian Institute of Technology, Guwahati, 2006.

[25] Knight CW, Hardy SJ, Lees AW, Brown KJ. Finite element modeling of strip curvature during hot rolling. Iron Making and Steel Making 2002;29:70–6.

[26] Gudur PP, Dixit US. A neural network-assisted finite element analysis of cold flat rolling. Engineering Applications of Artificial Intelligence, in press, doi:10.1016/j.engappai.2006.10.001.

[27] Dixit US, Dixit PM. An analysis of the steady-state wire drawing of the strain hardening materials. Journal of Materials Processing Technology 1995;47:201–29.

[28] Christensen P, Everfelt K, Bay N. Pressure distributions in plate rolling. Annals of CIRP 1986;35:141–6.